PERGAMON

Journal of Structural Geology 25 (2003) 1645–1658

JOURNAL OF STRUCTURAL GEOLOGY

www.elsevier.com/locate/jsg

Predicting reservoir-scale faults with area balance: application to growth stratigraphy

Richard H. Groshong Jr[a,*], Jack C. Pashin[b], Baolong Chai[c], Robert D. Schneeflock[d]

[a]*Department of Geological Sciences, The University of Alabama, Box 870388, Tuscaloosa, AL 35487-0338, USA*
[b]*The Geological Survey of Alabama, P.O. Box 869999, Tuscaloosa, AL 35486-6999, USA*
[c]*Slumberger/SIS, 5599 San Felipe, Suite 1700, Houston, TX 77056-2722, USA*
[d]*Paramount Petroleum, 230 Christopher Cove, Ridgeland, MS 39157, USA*

Received 15 December 2001

Abstract

A reservoir that appears to lack faults at one scale of resolution or at one sampling density may nevertheless contain faults that are below the resolution of the observations. The area–depth relationship from a balanced cross-section is shown to contain the necessary information for predicting the sub-resolution fault heave. Existing area–depth theory is extended to include growth units, allowing structural length and thickness changes to be separated from the depositional changes. The technique is validated with a numerical model of a growth full graben and a sand-box model of a half graben; then field tested in the Gilbertown graben, a growth structure within the regional peripheral fault trend along the northern margin of the Gulf of Mexico. A cross-section developed from wells alone is used to infer the abundance of sub-resolution faults by the area-balance technique. A small but significant amount of sub-resolution extension is predicted and then confirmed with a high-resolution seismic line.

Keywords: Normal faults; Sub-resolution faults; Growth faults; Area-balanced cross-sections

1. Introduction

A fault that is below the resolution of the observation technique, regardless of the technique used, is a 'sub-resolution' fault (Baxter, 1998). This is a generalization of the concept of a 'sub-seismic' fault, a term widely used for faults that are smaller than the resolution of a 2-D seismic reflection profile. The concept is also appropriate for faults that are too small to detect on conventional wire-line well logs and for unsampled faults that fall between wells or between 2-D seismic lines. Sub-resolution faults can be very important for a variety of reasons. At the reservoir scale, small faults may form either barriers or conduits within the reservoir and therefore greatly affect reservoir performance (e.g. Ellevset et al., 1998; Foley et al., 1998; Knai and Knipe, 1998; Manzocchi et al., 1998; Walsh et al., 1998). The magnitude and distribution of strain caused by small faults is of great importance to broader questions related to the origin and evolution of the large-scale structures that contain them (e.g. Marrett and Allmendinger, 1992; Groshong, 1996; Baxter, 1998). It has been proposed that the displacement on sub-resolution faults may add to the total displacement by an amount up to that carried by the visible faults, thereby potentially doubling the total extension (Kautz and Sclater, 1988; Walsh et al., 1991; Marrett and Allmendinger, 1992). A valid structural interpretation must, therefore, include the effects of all faults, including those that are too small to be resolved (Wu, 1993).

How to infer the presence and importance of sub-resolution faults remains a critical question. The abundance of sub-resolution faulting is controlled by the physical properties of the stratigraphy and the mechanics of deformation. Thus the prediction of the importance of sub-resolution faulting should ultimately be based on a model of the mechanical process. The construction of a mechanical model that will predict sub-resolution faults in a specific reservoir requires a detailed knowledge of the mechanical properties of the stratigraphy, the boundary conditions, and the fracture criterion, along with analytical

* Corresponding author. Tel./fax: +1-205-348-1882.
E-mail address: rgroshon@wgs.geo.ua.edu (R.H. Groshong).

0191-8141/03/$ - see front matter © 2003 Elsevier Science Ltd. All rights reserved.
PII: S0191-8141(03)00002-6

techniques that are capable of dealing with a high level of detail while remaining practical in application. Making specific predictions about individual field examples is often impossible because some of the required mechanical information is either not available or is not known to sufficient accuracy to make reservoir-specific predictions (Maerten et al., 2000). As a result, other approaches to the prediction of sub-resolution faults have been applied in an effort to make practical, reservoir-specific predictions.

One alternative is to greatly simplify the mechanical model. A kinematic model represents such a simplification in which a displacement field is specified (e.g. White et al., 1986; Wickham and Moeckel, 1997) without explicitly including all the boundary conditions or the mechanical properties of the material that combine to cause the displacement field. The value of kinematic models in geometric analysis is well documented. Kinematic models can also provide a quantitative link between the first-order structural geometry and the sub-resolution fault strain as shown by Groshong (1990) and Withjack et al. (1995). Unfortunately, even though a kinematic model may provide a good fit to one or more aspects of the geometry, it may fail to provide an accurate representation of the strain distribution at the scale of the sub-resolution faults (Chai, 1994; Chai and Groshong, 1994; Withjack et al., 1995).

Stochastic models take a different approach, one in which the sub-resolution faults are inferred to be the missing part of an otherwise continuous statistical size distribution. The model is used to extrapolate an observed fault population distribution to a different location or to a different size range at the same location (e.g. King, 1983; Childs et al., 1990; Scholz and Cowie, 1990; Marrett and Allmendinger, 1991, 1992; Walsh et al., 1991; Wu, 1993; Carter and Winter, 1995). The amount of layer-parallel strain that has been predicted as resulting from sub-resolution faults can be substantial, with estimates ranging from 25 to 60% of the total (Walsh et al., 1991; Marrett and Allmendinger, 1992). The relationships, however, are not necessarily invariant with respect to fault size or geographic location (King and Cisternas, 1991; Wojtal, 1994, 1996; Peacock and Sanderson, 1994; Brooks et al., 1996; Nicol et al., 1996; Gross et al., 1997). This renders problematical the predictions for structures for which a scaling relationship is not available.

A third approach is adopted here, the calculation of sub-resolution fault strain from an area-balanced cross-section. The distribution of area within a structure is the mechanical response to the process of deformation. The relationship between area and depth captures key aspects of the mechanical response without requiring knowledge of the specific process, the mechanical properties, or the stresses. If the locations of the boundaries between the deformed and the undeformed regions are known, the boundary displacement can be determined from the area–depth relationship and, from this, the original bed lengths. Original and final bed lengths are compared to determine layer-parallel extension. This extension provides the estimate of the heave on sub-resolution faults. Previous work (Hossack, 1979; Groshong and Epard, 1994; Groshong, 1994, 1996) has demonstrated that the area-balance strain calculation applies to area-constant pregrowth sequences in both compressional and extensional structures.

In this paper we extend the previous area-balance work to include the common situation of units that have variable thicknesses due to deposition during deformation. The necessary relationships are derived and verified by application to both analytical and experimental models. We conclude with a field example from the Gilbertown graben system, a large structure located along the northern margin of the Gulf of Mexico. A cross-section of the graben has been constructed from well-log data. This cross-section is not expected to resolve small faults, especially those occurring between wells. The area–depth relationship from the cross-section is used to predict the amount of extension due to sub-resolution faults. The prediction is corrected for the effects of compaction, as will usually be necessary in growth structures. The predicted extension is then compared with the measured results obtained from a high-resolution seismic line. The line shows faults not detected in the wells and the area-balance extension prediction is a remarkably close match to the additional fault extension seen on the seismic line.

2. Area-balance strain and fault prediction

Area balancing (Chamberlain, 1910) has traditionally been used to determine the depth to detachment (e.g. Chamberlain, 1910; Hansen, 1965; Gibbs, 1983; Groshong, 1996, and references cited therein). The procedure can be reversed, however, so that if the depth to detachment is known, it becomes possible to find the layer-parallel strain. The position of the lower detachment may be known either from direct observation or from the area intercept of the area–depth curve (Epard and Groshong, 1993; Groshong, 1996, 1999). Displacement on a lower detachment results in areas being uplifted or downdropped from their original elevations. The displaced area is the area enclosed between a given horizon in its deformed position and its original undeformed position (Fig. 1). The original regional elevation of a horizon before deformation is generally referred to simply as the *regional* (McClay, 1992). To find the layer-parallel strain in any unit, the following must be known: (1) the boundaries of the deformed area, (2) the regional, and (3) the position of the lower detachment. Area change caused by the deformation is not allowed, although stratigraphic thickness changes caused by variations in accommodation space are acceptable. Compaction due to the weight of the overburden will be considered later.

2.1. Area-balance strain

The displacement that formed the structure (D) is found

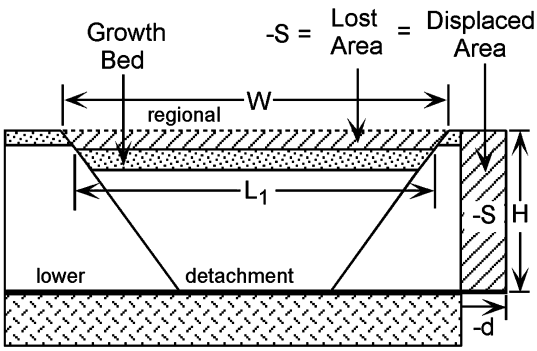

Fig. 1. Cross-section of an area-balanced full graben that includes a growth bed (dot pattern). The diagonally ruled areas are the displaced areas caused by an incremental displacement ($-d$) on the lower detachment.

from the displaced area (S) and the distance (H) between the lower detachment and the regional:

$$D = S/H, \tag{1}$$

where D is negative if extensional and S is negative if below regional. A lowercase d is used here for a post-growth displacement and an uppercase D for the total displacement; the equation has the same form for both. The length of a particular horizon as seen on a cross-section is its final length L_1, which may include bed-length changes. From the geometry of Fig. 1, the original length of the horizon (L_0) is:

$$L_0 = W + d = W + S/H \tag{2}$$

where W is the width of the structure at the regional of the horizon and d is the displacement of a growth horizon. The final dip of the horizon need not be horizontal as it is in Fig. 1 and the equation applies equally well to a half graben. W is always measured parallel to the regional and can be tilted if the regional is tilted. The value of L_0, calculated from the displaced area, is independent of the stratigraphic growth of the unit because it depends only on the length along the upper surface of the unit, not on the thickness. The bed-length change is:

$$\Delta L = L_1 - L_0 = L_1 - (W + S/H) \tag{3}$$

The length difference can be converted to layer-parallel strain, e, by dividing Eq. (3) by Eq. (2):

$$e = \left(\frac{HL_1}{HW + S}\right) - 1 \tag{4}$$

The computed value of ΔL or e is the *requisite* layer-parallel length change or strain, respectively, which is the amount required for the cross-section, as shown, to be area-balanced (Groshong and Epard, 1994; Groshong, 1994, 1996). Requisite length change and strain are so named in order to distinguish them from values that have been directly measured or inferred by some other technique.

2.2. Sub-resolution fault prediction

Sub-resolution faults will change the apparent geometry of a bed in different ways, depending on the resolution of the observations. Consider a faulted bed in which all the faults are perfectly resolved (Fig. 2a). The final length (L_1) of the deformed unit is the sum of the original bed lengths between the faults (L_0), plus the sum of the layer-parallel components of displacement on all the faults (D). Now consider the effects of differing levels of resolution on the observed geometry. At low resolution, the shape of a faulted bed might be given either by a curved-bed approximation (Fig. 2b), for which the apparent bed boundaries include parts of the fault traces (Fig. 2c), or by an average-surface approximation (Fig. 2d), for which the apparent bed boundaries smooth out the fault offsets to approximate a plane bed (Fig. 2e). For low-resolution observations (Fig. 2c and e), the apparent bed length L_1 will be equal to or even greater than the length that includes the original bed length plus the total extension, for which $L_1 = L_0 + D$. The opposite will be true if the bed is shortened; it will appear shorter than its original length.

The amount of extension or contraction of a bed cut by sub-resolution faults can be given as the change in bed length:

$$\Delta L = L_1 - L_0, \tag{5}$$

or as a layer-parallel strain, e:

$$e = \Delta L/L_0 = (L_1/L_0) - 1, \tag{6}$$

for which extension is positive and contraction negative. If the bed-length change is accomplished by faults, as in Fig. 2, then the number of faults of a given size that are required to accomplish a particular layer-parallel extension or contraction can be estimated. In cross-section, the layer-parallel displacement caused by one fault is δL, the layer-normal displacement is δv, the dip of the fault is θ, and $\tan\theta = \delta v/\delta L$, where all measurements are made in coordinates parallel and perpendicular to layering. The total bed-length change is $N\delta L$, where N is the number of faults. From the definition of strain (Eq. (6)), the layer parallel strain is:

$$e = N\delta L/L_0 = N\delta v/L_0 \tan\theta, \tag{7}$$

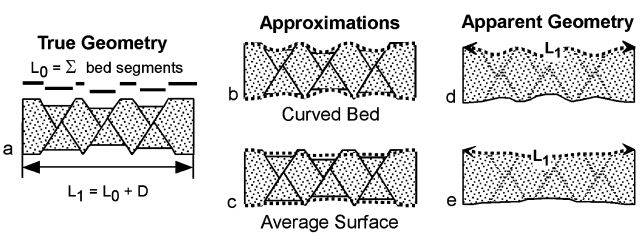

Fig. 2. Representative segment of a bed deformed by distributed normal faulting. The total extension of each is identical. (a) Constant bed length deformation on discrete, resolvable faults. (b) Curved-bed approximation to the faulted surfaces. (c) Average-surface approximation to the faulted surfaces. (d) Apparent geometry of curved-bed approximation. (e) Apparent geometry of average-surface approximation. L_0 = original length of bed, L_1 = final length of bed, D = sum of layer-parallel component of fault displacements.

which is solved for N to give:

$$N = (eL_0\tan\theta)/\delta v, \quad (8)$$

or, in terms of the total bed-length change, ΔL:

$$N = (\Delta L\tan\theta)/\delta v. \quad (9)$$

As an example of the number of sub-resolution faults required to accomplish a given extension, suppose the smallest resolvable fault throw is 30 m (a typical value for a 2-D petroleum-industry seismic line), the total extension is 0.10 (10%), the fault dip is 60°, and the original bed length is 1 km. From Eq. (9), $N = 5.8$ sub-resolution faults per kilometer of original bed length will produce 10% extension. This is the minimum number of sub-resolution faults required for the given amount of strain. A larger number of smaller faults could accomplish the same amount of strain.

3. Area-balance strain prediction applied to models

To illustrate and confirm the area–depth prediction of bed-length change, the technique is applied to a numerical model of a growth full graben and to an experimental model of a half graben. In addition, the numerical model provides an example of the complete area–depth analysis of the cross-section of a growth structure. Measurements of lengths and areas are done utilizing the program Canvas (Groshong and Epard, 1996). The measurements are accurate to three significant figures. Requisite strains as percentages measured in Canvas are accurate to about ± 2–3 tenths of a percent.

3.1. Numerical experiment

The area–depth-strain relationships in a growth graben system are first illustrated by application to an analytical area-balanced forward model of a full graben (Fig. 3). The model represents pure-shear extension above a planar detachment in which the original graben area remains constant, expanding laterally and subsiding uniformly to remain in contact with the lower detachment and with the footwall blocks as they move apart. Beds are horizontal both before and after deformation. The strain in the graben is a downward-increasing, horizontal, pure-shear extension. Field examples of detached full grabens are relatively common, for example, in the Appalachian Black Warrior basin (Groshong, 1994) as well as along the up-dip rim of the Gulf of Mexico (the Gilbertown graben example later in this paper). The model was constructed by incrementally extending the cross-section while maintaining the original area of the graben trapezoids bounded by the regional, the lower detachment and the bounding faults for the top of each unit in the graben. The faults form and propagate with a dip of 60°. The pregrowth sequence (Fig. 3a) consists of units with thicknesses that were constant prior to extension. Growth sediments are deposited in steps (b)–(f), overfilling the graben in each step and producing a horizontal upper surface. Compaction is not included in the model. An increment of displacement without deposition in step (g) completes the model. All units within the graben are stretched and structurally thinned in the process of graben formation. The extension and thinning are obvious in the pregrowth units by a simple visual comparison between Fig. 3a and g. The thinning is masked in the growth units by the depositional thickening, but layer-parallel extension is nevertheless present. The model represents the deformation as being homogeneous at the bed scale.

To illustrate the technique and demonstrate its validity, the layer-parallel extension of the growth bed deposited in step (e) (Fig. 3) is determined from its original and final bed lengths, and this 'ground-truth' value is compared with that determined from the area-balance of the final-stage cross-section alone (Fig. 3g). The two stages are shown separately and the measurements labeled in Fig. 4. The direct measure of L_0 for horizon 2 is the bed length at the surface between the projections of the two boundary faults (Fig. 4a). The final bed length, L_1, is measured directly in Fig. 4b. The strain of horizon 2 is then found from Eq. (6) to be 3.1% layer-parallel extension. The requisite strain for horizon 2 is obtained from measurements made only on the final deformed state cross-section (Fig. 4b) and calculated from Eq. (4). The result is a requisite extension of 2.8%. The difference between the two values (0.3%) represents the accumulated measurement errors, not a significant difference, thereby confirming the area–depth relationship for strain calculation. The complete area–depth relationship for the model is given in Appendix A.

3.2. Physical experiment

The requisite-strain calculation is next tested with an experimental sand-box model of a half graben (Fig. 5). This test shows that the technique is not restricted to analytical models or to full grabens. The hanging wall of the normal fault in the model has been displaced along a pre-formed listric fault. Following the experimental design of McClay and Ellis (1987), a mylar sheet at the base of the sand is attached to the moving wall in order to ensure that the entire hanging wall shares in the displacement. The experimental material is well-sorted dry sand of 350 μm grain size. The dark layers consist of colored sand of the same size. Measurements on the whole model reveal that the entire model has been extended, not just the region over the curved portion of the fault, and that there is an area increase of 5.6 cm^2 or 2.5% caused by the deformation (Chai, 1994). An area increase is expected because the sand grains change to a looser packing arrangement during deformation. The sand was not compacted during model construction and so the area increase is small. The uppermost dark band in the model was extended 10.8% in the rollover, as determined by locating the hinge point in the model relative to

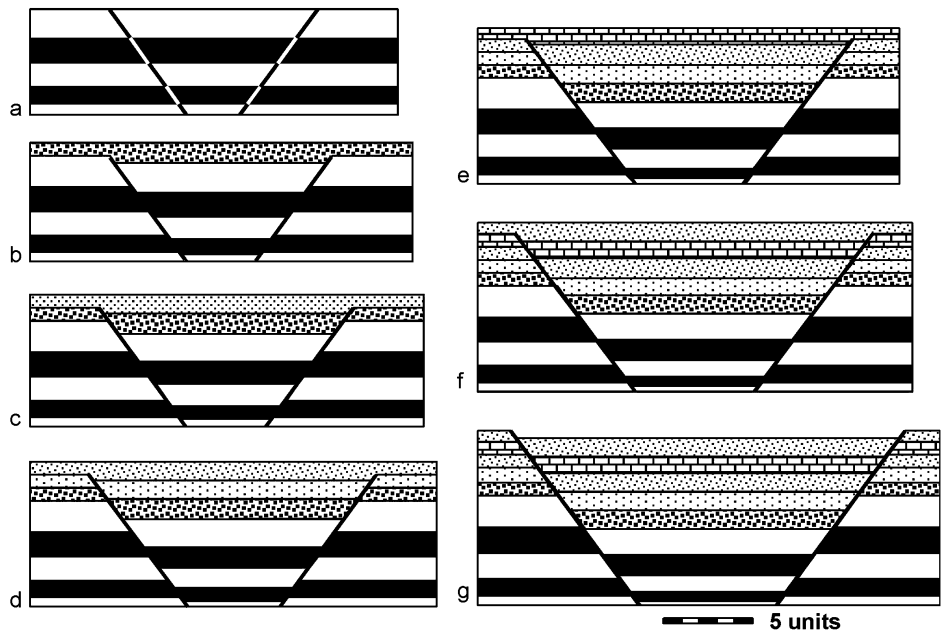

Fig. 3. Area-constant forward model of a growth graben. Pregrowth beds are solid black or white, growth beds are patterned. (a) Before deformation, zero displacement. (b)–(g) Sequential extension and deposition of growth beds. Displacement increments: (a)–(b) 0.5 units; (b)–(c) 1.0 units; (c)–(d) 0.5 units; (d)–(e) 1.0 units; (e)–(f) 0.5 units; (f)–(g) 1.0 units.

pre-deformation markers and measuring the bed length between the hinge point and the fault before and after deformation (Chai, 1994).

Here we interpret the model as if it were a field example for which only the deformed state is known. The measurements are shown in Fig. 5. Uncorrected for area increase, the requisite strain from Eq. (4) is 8.3% extension along the top bed in the rollover. The deformation-induced area increase of the model reduces the lost area in the graben, relative to a constant-area-model. Correcting for the area increase by assuming that all the increase occurred entirely in the rollover has the effect of reducing the lost area of the graben by 5.6 cm^2, and the requisite strain in the rollover (Eq. (4)) would then be 12.7% extension. Deformation occurred throughout the entire model, not just in the rollover (Chai, 1994), and so the deformation-related area change should also be distributed over the entire model, not just restricted to the rollover. The reduction of lost area in the graben caused by the area increase of the sand should therefore be somewhat less than 5.6 cm^2 but more than zero. Thus the true amount of requisite strain must lie between the corrected (12.7%) and uncorrected (8.3%) values. The average of the two values is 10.5%, very close to the layer-parallel extension in the rollover determined by direct measurement on the entire bed (10.8%). This confirms the ability of the lost-area calculation technique to determine the sub-resolution strain to a relatively high degree of accuracy.

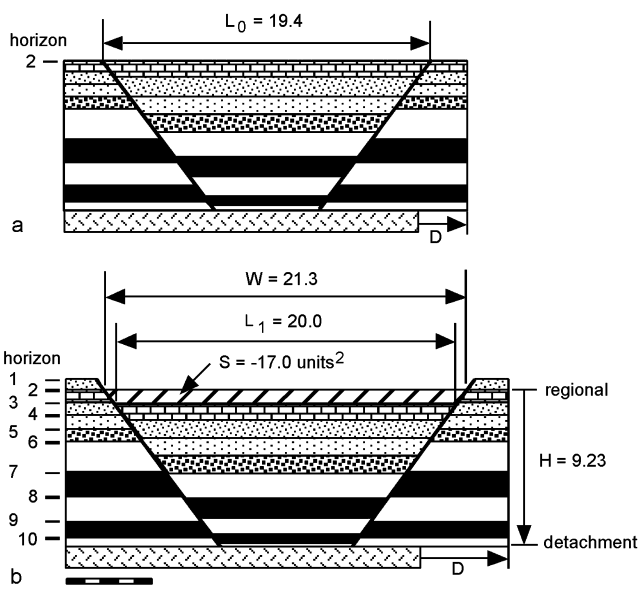

Fig. 4. Data for area balance and strain calculation for a growth unit in the full graben model. (a) Cross-section from Fig. 3e, representing the geometry at the time of deposition of horizon 2. (b) Cross-section from Fig. 3g, representing the geometry after deposition of horizon 1 and an additional increment of displacement. Diagonal pattern is the lost area of horizon 2. Scale bar is 5 units.

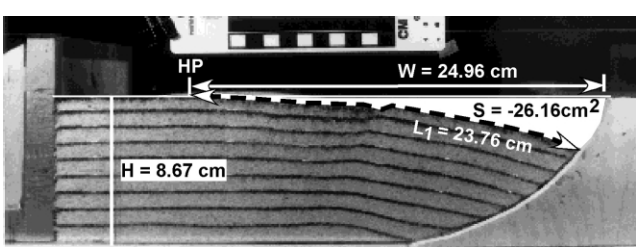

Fig. 5. Experimental model of a half graben (after Chai, 1994). The hanging wall is homogeneous sand with lines of dark sand as marker layers. The scale divisions are 1 cm, HP = hinge point.

4. Sub-resolution faulting in the Gilbertown graben

We now apply the area–depth relationship to predict the sub-resolution faulting in a large field example. The structure is the Gilbertown Graben system located in southern Alabama (Fig. 6). This structure is particularly suitable for a test of the technique because an interpretation based exclusively on well logs (Pashin et al., 2000) was completed prior to a 3-D seismic survey becoming available over a portion of the area. The original well-based interpretations can thus be compared with the 3-D seismic interpretation in a completely independent test.

The Gilbertown graben system occurs near the updip limit of salt along the regional peripheral fault trend of the Gulf Coast basin. Down-dip gliding on the salt is the probable cause of the extension at this location (Cloos, 1968). The salt can be identified on seismic lines as pinching out in the vicinity. The graben system is developed between the north-dipping West Gilbertown and Langsdale faults and the south-dipping West Melvin fault (Fig. 6). The Gilbertown oil field occurs parallel to the trace of the West Gilbertown fault. Reservoirs in this field are Cretaceous in age and occur in glauconitic sandstone of the Eutaw Formation in the footwall and the fractured chalk of the Selma Group in the hanging wall (Current, 1948; Braunstein, 1953; Bolin et al., 1989; Pashin et al., 2000). Because the permeability of the Selma chalk is entirely a function of fracturing, the presence or absence of sub-resolution faults has a practical as well as a theoretical significance.

4.1. Cross-section

The cross-section (Fig. 7) is controlled by a regional 3-D model and locally by the wells closest to the line of section. The 3-D interpretation of the graben system was developed in GeoSec3D using the logs from over 625 wells (Pashin et al., 2000). Within a given fault block the thickness of most units is nearly constant in adjacent wells. Thus, in the interpretation process, stratigraphic thicknesses were maintained as constant as possible where horizons were projected into faults. All mappable fault surfaces were intersected with multiple stratigraphic horizons in order to ensure the internal consistency of both the beds and the fault surfaces, following the methods of Groshong (1999). To be mapped we required that a fault be found in more than one well. This criterion leads to the omission of small faults and faults on the edges of the data set, in other words, it allows sub-resolution faults to be present. In the vicinity of the cross-section, the structure of the Selma Group and the Eutaw Formation is controlled by numerous wells. The deep structure is controlled by a few key wells and by the stratigraphic separations on faults. We retain the original units (feet) on the cross-section and on all measurements in order to retain the original accuracy of the measurements (1 m = 0.3048 ft).

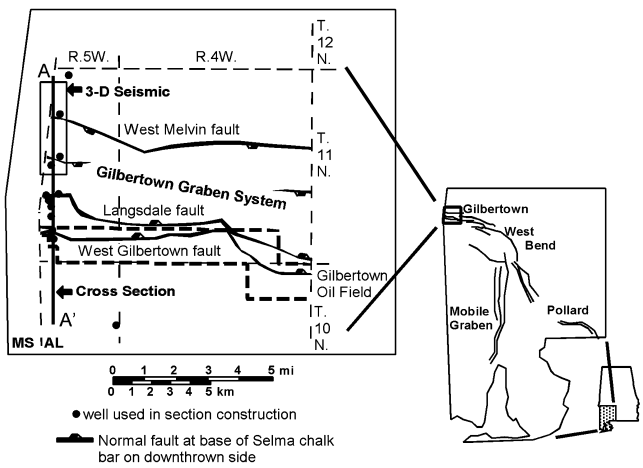

Fig. 6. Index map to the western part of the Gilbertown graben system. Faults are shown as they occur at the top of the Selma Group (after Pashin et al., 2000). Cross-section A–A′ is given in Fig. 7. Thick dashed lines show the boundary of the Gilbertown oil field.

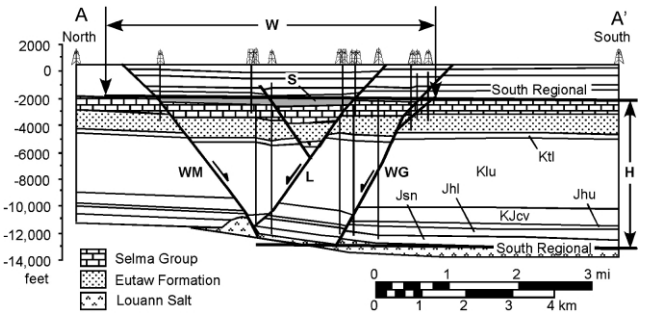

Fig. 7. Cross-section A–A′ from the Gilbertown graben system (after Pashin et al., 2000). The location of the cross-section is shown in Fig. 6. No vertical exaggeration. The width (W) of the graben at the top Selma is shown. S = lost area of Selma, H = distance between top of Selma and detachment, WM = West Melvin fault, L = Langsdale fault, WG = West Gilbertown fault. Units between the Eutaw Formation and the Louann Salt are, from youngest to oldest, Ktl = lower Tuscaloosa Group, Klu = Lower Cretaceous undifferentiated, KJcv = Cotton Valley Group, Jhu = upper Haynesville Formation, Jhl = lower Haynesville Formation, Jsn = Smackover and Norphlett Formations.

Regionally, the shallow-marine Smackover through Cotton Valley Formations maintain relatively constant thickness and so are interpreted as forming the pregrowth stratigraphy (Fig. 7). This interpretation does not rule out minor amounts of growth below the resolution of the cross-section. The graben began to form during the deposition of the lower Cretaceous clastic sequence, as demonstrated by the substantial expansion of section across the master faults. A downward shift of the hanging wall regional across the graben is apparent in the KJcv and older units on the south side of the cross-section (Fig. 7). This downward shift could be caused by either salt withdrawal from the south side or displacement on a lower detachment that dips south at a low angle, which is steeper than the dip of bedding. Regional seismic lines show no evidence of a low-angle fault below the Louann salt, implying that the lower detachment is in the salt. Depth-to-detachment determinations from multiple

cross-sections across the fault system also indicate that the lower detachment is in the salt (Pashin et al., 2000). See Appendix B for a model of the kinematics and area balance of the salt evacuation. Salt that evacuated from adjacent to the Gilbertown graben system migrated laterally to the south to form the Hatchetigbee anticline, a turtle structure (Pashin et al., 2000). Regional elevations of horizons are relatively constant across the graben at the top of the lower Cretaceous Ktl and for all younger units, indicating that salt withdrawal had ceased and that extension during deposition of the Eutaw and Selma occurred on a bedding-parallel lower detachment in the salt.

Here we focus on the faults in the Selma Group and Eutaw Formations because the well control is best for these units and because they produce the clearest (highest amplitude, most continuous) reflectors on the 3-D seismic profile, allowing a detailed comparison between the cross-section and the seismic profile. The units are nearly horizontal, and as a result the horizontal component of fault separation is equal to the fault heave. The measured heaves on individual faults and the total heave are given in Table 1.

4.2. Fault prediction from area–depth relationship

Predicting the abundance of sub-resolution faults from the area–depth relationship requires selecting the appropriate regional elevations, locating the lower detachment, and making a correction for compaction before performing the final calculation. Because of the salt-related subsidence of the south flank of the graben, the south-side regionals are appropriate. The area-balance of the graben is not affected by the salt-related subsidence as long as the subsided regional is selected (Appendix B). The lower detachment is placed at the top of the salt, based on the results of the area–depth graphs of all the cross-sections constructed by Pashin et al. (2000) and results given in Appendix B. The areas and length parameters are measured directly in Fig. 7 and given in Table 2.

Compaction can have an important effect on the lost areas of growth units. Without correction for compaction, the calculated requisite strains for the cross-section are small negative numbers, which implies layer-parallel contraction in the graben. This is not a realistic result in an extensional environment and underscores the need for the compaction corrections. The measured lost area must be corrected for both regional compaction and for differential compaction caused by the greater thickness of sediments in the graben. The details of the compaction corrections are given in Appendix C and the results summarized in Table 3. The constants in Table 3 are the values for chalk (Selma) and shaley sand (Eutaw) given by Sclater and Christie (1980) except that the final porosity (ϕ_1) of the Eutaw is estimated from local well data. The average porosity of Eutaw reservoir sandstone calculated from well logs by Pashin et al. (2000) for the Gilbertown area is $\phi_1 = 0.255$ and the shale porosity, although unmeasured, is perhaps a tenth of that amount because the shale is the seal for oil reservoirs in the sandstone. Shale constitutes on the order of half the formation, giving an estimate of the final bulk porosity of 0.14, the value given in Table 3.

Table 1
Measured fault heaves (ft) on unit tops, measured on cross-section section A–A′ (Fig. 7). WM = West Melvin fault, N = northern unnamed fault, L = Langsdale fault, WG = West Gilbertown fault, S = southern unnamed fault

Unit	WM	N	L	WG	S	Total (ft)
Selma	90	60	170	70	–	410
Eutaw	120	170	230	30	60	610

Table 2
Area–depth measurements on cross-section A–A′ (Fig. 7)

Unit top	Lost area (ft^2)	H (ft)	W (ft)	L_1 (ft)
Selma Group	−7,560,000	10,800	24,100	23,200
Eutaw Formation	−7,000,000	9680	22,500	21,600

The compaction-corrected lost areas, requisite strains and length changes are given in Table 4. Requisite strain and length change are obtained from Eqs. (3) and (4) using the net lost area. The requisite strains and length changes represent small but significant extensions (Table 4). The greatest numerical uncertainty in the strain and length-change calculation is in the compaction correction. Greater compaction will result in greater amounts of requisite extension. To judge the sensitivity of the requisite strain and length changes to the amount of compaction, the compaction values (C) have been changed ±25% from the values in Table 3. For the Selma this causes the requisite strain to range from 0.1 to 1.5% and the requisite length change to be 35–240 ft. For the Eutaw this causes the requisite strain to range from 0.7 to 3.4% and the requisite length change to be 150–711 ft. These ranges are comparable with the ranges estimated from the seismic reflection profiles (Table 5). The requisite extension calculated from the cross-section could represent a homogeneous strain within the beds, heave on unrecognized faults, or some combination of the two.

The plus and minus values given for the requisite strains and requisite length changes in Table 4 are the amounts associated with the probable measurement errors. The value of 0.3% requisite strain difference, interpreted as a difference due to cumulative measurement errors in the numerical model, is thought to be a reasonable estimate of the measurement error. It is applied here as giving a range of ±0.15% on the measured values.

4.3. Faults observed on 3-D seismic

A seismic line (Fig. 8) has been selected from a 3-D survey at a location close to the cross-section of Fig. 7. The

Table 3
Data for compaction corrections for the Gilbertown cross-section A–A′ See Appendix C for an explanation of the symbols

Unit	Midpoint depth (ft)	W_b (ft)	L_b (ft)	t (ft)	t_g (ft)	ϕ_0	c (km^{-1})	ϕ_1	C	$D.R.$
Selma	2560	13,800	12,200	1050	1160	0.68	0.47	0.51	0.39	1.64
Eutaw	3800	12,200	10,100	1250	1390	0.56	0.39	0.14	0.41	1.69

line crosses approximately the north half of the graben at the level of the Selma and Eutaw (Fig. 6). The top of the Selma Group and the top of the Eutaw Formation produce seismic reflections that can be unambiguously correlated to the well logs.

The seismic profile reveals a number of small faults that were not interpreted on the cross-section (Fig. 8b), and somewhat different heaves on the faults that are on the cross-section. Four new faults were discovered in the Selma Chalk with a total of 90 ft of heave and the Eutaw Formation shows six new faults (one of which also cuts the Selma) with a total heave of about 270 ft. Where the fault throw is clear but the fault itself is not, the fault heave is based on the observation that most well-documented faults in this area dip about 60°.

4.4. Comparison between predictions and observations

Because the seismic line crosses only the northern half of the graben, it presumably records only part of the total sub-resolution fault heave predicted from the area-balance of the whole graben. If the sub-resolution faults are equally distributed across the graben, then the seismically observed fault heave should be doubled to represent the entire graben. The southern half of the graben, not sampled by the 3-D survey, includes the Gilbertown oil field where the structure is better controlled by closer well spacing than in the area of the seismic survey. Thus the southern half of the graben should contain fewer sub-resolution faults than the northern half. A range of extension from an amount equal to that on the seismic line to twice that on the seismic line is reasonable for the amount of sub-resolution fault heave for the whole cross-section (Table 5). The predicted values of sub-resolution extension for both the Selma and the Eutaw are in the middle of the range of the additional heave observed on the seismic profile. Thus the predictions are consistent with the observations.

5. Discussion

Insight gained from the seismic profile shows that the construction of cross-section A–A′ underestimated the presence of small faults and faults on the edge of the data set. The small panel of south dip in the center of the cross-section should have been interpreted as a fault offset. The northernmost fault seen on the seismic line, in the footwall of the Melvin fault, was observed in one well but could not be found in any other well and so was not shown on the section. Because all the localized elevation changes are evidently the result of faults, the stratigraphic sequence is clearly very brittle. This is true even though stratigraphic growth in both the Selma and the Eutaw shows that they were deformed while very young and at shallow depth.

The Gilbertown graben in cross-section A–A′ (Fig. 7) is a full graben containing nearly horizontal beds and represents a structural style to which the most commonly used kinematic models do not apply. The kinematic models most commonly applied to extensional structures, e.g. oblique simple shear, flexural slip, and rigid-body displacement (Groshong, 1999), predict zero layer-parallel extension for horizontal beds. Oblique simple-shear models require a dip change of bedding for strain to develop. Flexural-slip models maintain constant bed length, regardless of dip. Of course, by definition, a rigid-block displacement model does not include layer-parallel strain between the faults. The graben has a small but significant amount of layer-parallel extension at the shallow levels where the Selma Chalk and the Eutaw Formation are located. The amount of layer-parallel extension could be much greater at deeper levels where the graben must widen at its contact with the lower detachment. As shown by the area-balanced pure-shear model (Fig. 4 and Appendix A), if the beds remain horizontal as the detachment is approached, very large strains are required. The lack of a large amount of small-scale faulting at the Selma and Eutaw levels in the Gilbertown graben does not preclude the occurrence of many more sub-resolution faults deep in the graben.

Table 4
Calculated values for the Gilbertown cross-section A–A′

Unit top	Decompacted lost area (ft)	Lost area of differential compaction (ft^2)	Net lost area (ft^2)	L_0 (ft)	Requisite e (%)	Requisite ΔL (ft)
Selma	−12,393,443	+914,262	−11,479,180	23,037	0.7 ± 0.15	163 ± 24
Eutaw	−13,725,490	+1,499,784	−12,225,706	21,237	1.7 ± 0.15	363 ± 54

Table 5
Predicted sub-resolution fault heave and seismically observed fault heave

Unit	Fault heave (ft)	
	Predicted requisite extension	Additional heave from 3-D seismic profile (observed and 2 × observed)
Selma	163 ± 24	90–180
Eutaw	363 ± 54	270–540

If the fault-size scaling relationship given by Walsh et al. (1991) applies to this structure, their figures indicate that 40% of the extension seen on the visible faults could be present on sub-resolution faults. Forty percent of the extension on the mapped faults (Table 1) is 164 ft for the Selma Chalk and 244 ft for the Eutaw formation. The total extension on sub-resolution faults predicted from the scaling relationship is nearly the same as from the area balance and falls within the range of observed values (Table 5), indicating that the Walsh et al. (1991) scaling relationship might apply to the Gilbertown graben.

Could substantially more fault displacement occur on cross-section A–A′ below the resolution of the seismic line? The general agreement of the area-balance prediction with the seismic observations suggests that the 3-D seismic profile has detected essentially all the sub-resolution extension on cross-section A–A′ If even smaller sub-resolution faults exist, their total heave should be very small. High-resolution SCAT analysis (Groshong, 1999) of the few dipmeter logs that are available in the Gilbertown oil field on the south side of the graben indicates that additional small faults occur very close to the master faults (Jin et al., 1999; Pashin et al., 2000). At the scale of cross-section A–A′, the heave on these sub-resolution faults is included with that of the master faults and therefore does not appear in the requisite strain calculation. SCAT analysis indicates essentially no faulting in most wells away from the master faults.

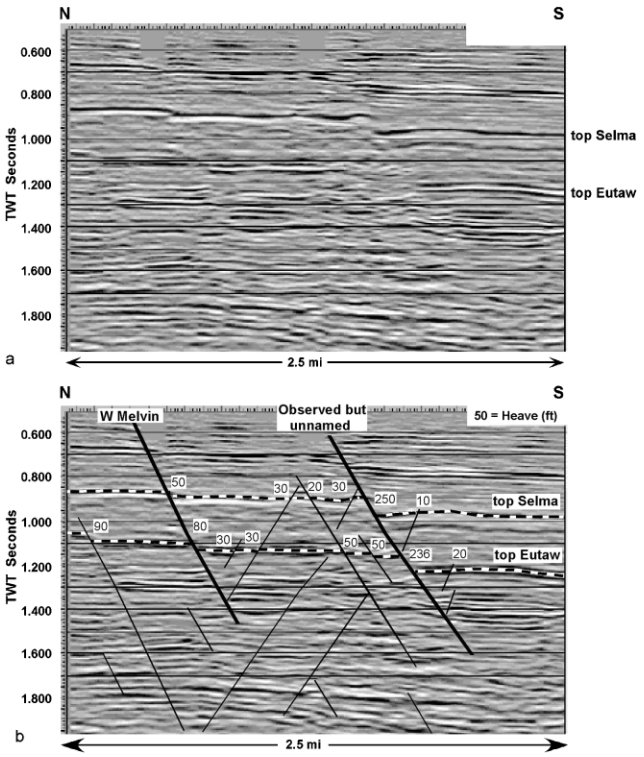

Fig. 8. Seismic reflection profile corresponding approximately to the northern half of cross-section A–A′ (Fig. 7). It is a time-migrated profile from a 3D data survey. V.E. about 1:1. (a) Uninterpreted. (b) Interpreted. The faults indicated with heavy lines are also recognized in Fig. 7. The numbers next to the faults are fault heaves in feet. Only the most obvious faults are interpreted below the top of the Eutaw because faults at deeper levels do not influence the results in this paper.

6. Conclusions

The geometry of a cross-section contains the information necessary to predict the magnitude of sub-resolution fault extension using the area–depth–strain relationship. Layer-parallel strain can be predicted from a cross-section based on measurements of bed length, width of the structure at regional, displaced area, and depth to detachment. The method applies directly to pre-growth units and, when corrected for compaction, applies to the growth beds as well. With this method, no assumptions are required about the mechanical properties of the stratigraphy, the kinematic model, or the fault scaling relationship. In order to apply the method, the horizons of interest must return to their regional elevations on at least one side of the structure and the position of the lower detachment must be known. The requisite strain represents the total layer-parallel strain over the length of the displaced bed and hence can be directly compared with the total sub-resolution fault heave. The method is illustrated and confirmed with both a numerical and a physical model. Although the technique is presented here in the context of structures formed in extension, it is equally applicable to structures formed in contraction.

The method is field tested with a cross-section across the Gilbertown graben system, a growth structure formed at the approximate up-dip limit of the salt along the northern margin of the Gulf of Mexico. The section was constructed from good well control and the calculations show small requisite extensions in the Selma Group and the Eutaw Formation, both growth units. The predicted extensions are small compared with the length of the cross-section but represent a significant amount of heave when compared with the observed fault heave. The predictions have been

tested utilizing an independent data set provided by a seismic reflection profile in which the tops of the Selma and the Eutaw produce good reflectors. The additional fault heave that is seen on the seismic line is nearly the same as that predicted from the area-balance model.

The distribution of excess or lost area on a cross-section contains sufficient information to allow the accurate prediction of sub-resolution fault strain. The closer a cross-section of brittle rocks is to being perfect, in the sense of showing all the faults, the smaller will be the predicted requisite strain. The area-balance approach can provide an independent check on the predictions made by other methods.

Acknowledgements

Partial funding for this research was provided by the U.S. Department of Energy through BDM-Oklahoma, Inc. subcontract No. G4S51733, Contract No. DE-AC22-94PC91008. A 3-D model of the Gilbertown graben based on wells that helped in cross-section construction was developed by Guohai Jin using GeoSec2D and GeoSec3D provided by Paradigm Geophysical Ltd. We greatly appreciate both Jin and Paradigm Geophysical for their help. We thank Dennis Harry for his assistance in the seismic interpretation and for his helpful comments on an earlier draft of this manuscript. The comments of two anonymous reviewers contributed significantly to the readability of the final manuscript.

Appendix A. Area–depth–strain relationship for analytical model

The complete area–depth graph of the analytical model in Fig. 4b (Fig. A1) illustrates the properties of a cross-section that includes growth and pregrowth units (Groshong and Pashin, 1997; Groshong et al., 2001). The reference level has been placed at the top of the cross-section, at the regional elevation of horizon 1. The boundary between the growth and pregrowth intervals is clearly identified by the sharp inflection point in the area-depth graph at the position of horizon 6. The points representing the pregrowth interval fall on a straight line because they all have the same displacement. The inverse slope of the best-fitting straight line (−4.5 units) is the total displacement on the lower detachment used to generate the model. The point at which the lost area goes to zero is the location of the lower detachment (−9.62 units below the reference level), which is the position of the lower detachment in the model. The growth beds (horizons 1–5) have lost areas that decrease upward (Fig. A1). The lost area of the youngest bed is not zero because an increment of extension has occurred after the deposition of this unit. The total displacements have been determined from Eq. (1), given the position of the lower detachment (Table A1), and match the input values.

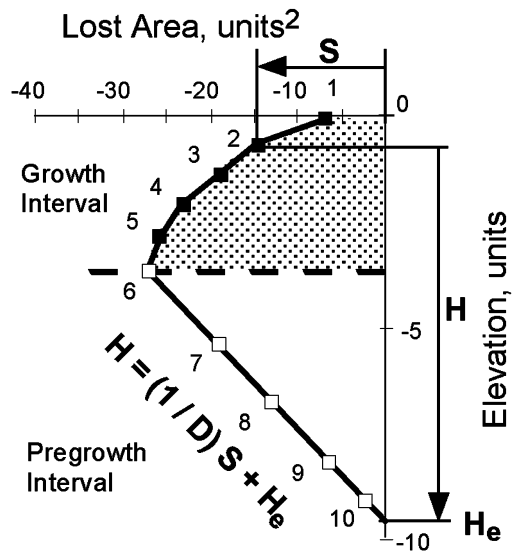

Fig. A1. Area–depth graph of the model in Fig. 4b pointing out the values for horizon 2. S = lost area, H = depth to detachment for a particular horizon, D = displacement of pregrowth units, H_e = elevation of the lower detachment.

The layer-parallel requisite strain for the model in Fig. 4b, calculated from Eq. (4), is an extension that increases downward in the graben to a maximum at the lower detachment (Table A1). The layer-normal strain, e_n, is:

$$e_n = (t_1/t_0) - 1. \tag{A1.1}$$

For constant area:

$$t_1 L_1 = t_0 L_0, \tag{A1.2}$$

where t_0 and t_1 are the thicknesses before and after deformation, respectively. The value of e_n can be found in terms of the layer-parallel requisite strain, e (Eq. (4)), by substituting Eqs. (6) and (A1.2) into Eq. (A1.1) to obtain:

$$e_n = -e/(e+1). \tag{A1.3}$$

The pregrowth sequence is significantly stretched horizontally and thinned vertically by the deformation, as is obvious on the cross-section. The growth sequence includes depositional thickening, which is greater than the structural thinning, giving a net thickness increase in each growth unit. The structural thinning can be recognized from the area balance (Eqs. (4) and (A1.3)) in spite of the net thickness increase because the lost area and hence the strain is a function only of the displacement and the depth to detachment.

Appendix B. Model of extension plus salt withdrawal

Withdrawal of salt from beneath one side of a graben

Table A1
Structural data calculated from the full graben model in Fig. 4b

Unit top	Total displacement (units)	Layer-parallel requisite strain (%)	Layer-normal requisite strain (%)
1	1.0	+0.9	−0.9
2	1.5	+2.6	−2.5
3	2.5	+4.6	−4.4
4	3.0	+7.0	−6.5
5	4.0	+10.3	−9.3
6	4.5	+15.2	−13.2
7	4.5	+24.0	−19.4
8	4.5	+37.5	−27.3
9	4.5	+66.2	−39.8
10	4.5	+104.2	−51.0

(Fig. A2a and b) along with extensional displacement produces two components of deformation in the graben, a rigid-block displacement associated with the salt withdrawal, and an internal strain associated with extension. The rigid-block component causes a change in the elevation of the regional. The internal strain component is obtained from the area–depth relationship of the graben using the displaced regional. Construction techniques used to produce the model are identical to those used to create Fig. 3 with the addition of salt-related subsidence.

The model (Fig. A2a) begins with a layer of salt of uniform thickness beneath one side of the future graben. This is believed to resemble the geometry of the Gilbertown graben system before extension and salt movement. Extension coupled to salt withdrawal (Fig. A2b) causes both the graben and its adjacent footwall to subside.

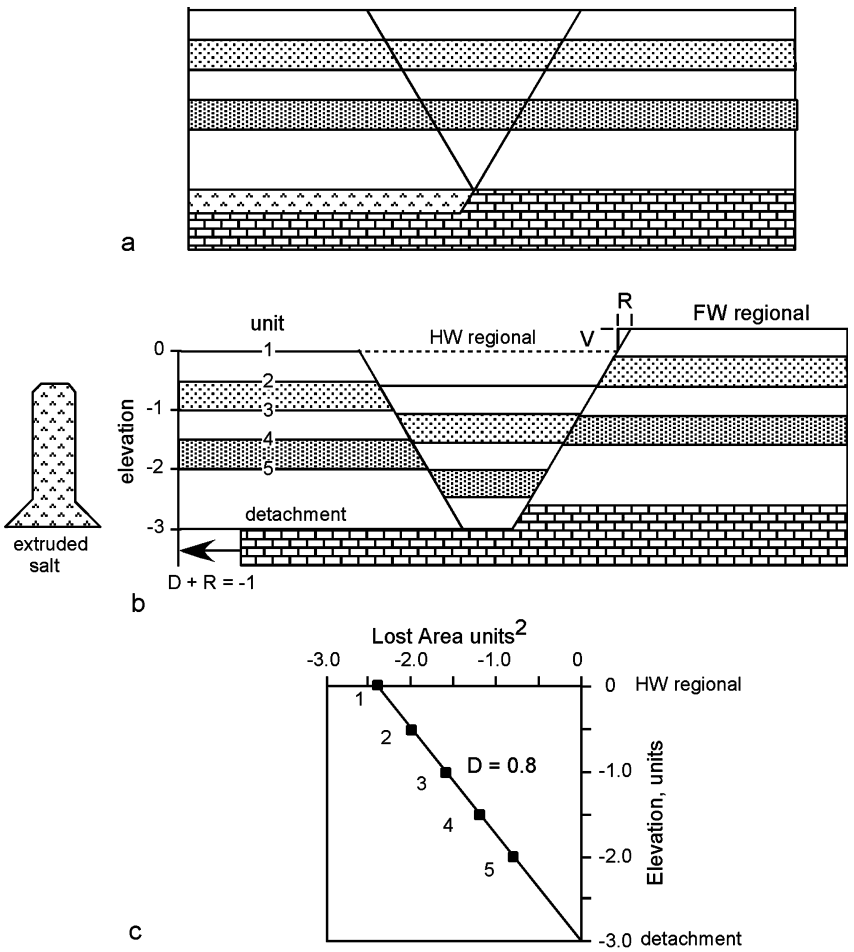

Fig. A2. Full graben associated with withdrawal of salt (^ pattern) plus extension. (a) Undeformed. (b) After 1 unit of extension and salt extrusion. Extruded salt is removed from the cross-section. HW = hanging wall, FW = footwall of master fault. (c) Area–depth diagram based on hanging wall regional projects to zero area at detachment.

Additional subsidence of the graben is caused by pure shear thinning within the graben. We refer to the subsided region as the hanging wall of the resulting graben system, the unsubsided region as the footwall of the system (Fig. A2b), and the fault that separates them as the master fault. The difference in elevation of the regionals across the master fault is the vertical component of the rigid-block displacement (throw) due to salt withdrawal. The horizontal component (heave) depends on the dip of the master fault and is:

$$R = V\tan\phi \tag{A2.1}$$

where R is the horizontal component of displacement, V is the vertical component of displacement, and ϕ is the fault dip (Fig. A2b).

The properties of the graben are defined on an area–depth graph that uses the hanging wall regional (Fig. A2c). In the model, the area–depth relationship is a straight line because only pregrowth units are present. The line projects to zero area at the inferred location of the lower detachment. This is the elevation of the top of the evacuated salt or, equivalently, the base of the rigid block that forms the subsided boundary of the graben. The inverse slope of the area–depth line, D, gives the displacement associated with the internal strain of the graben beds. The total bed-parallel displacement across the graben system is the sum of the rigid-block component, R, and the extensional displacement of the graben, D. The requisite strains within the graben could be calculated from the area–depth relationship, exactly as done for the example in Fig. 4.

Appendix C. Compaction corrections

The effect of compaction on the lost area can be important for growth units. The total effect of compaction includes two components, a lost-area decrease due to the uniform compaction of the unit containing the graben (Fig. A3a and b), and a lost-area increase due to differential compaction of the thicker sequence in the graben relative to the thinner sequence outside the graben (Fig. A3c). The lost area of the graben in the uncompacted unit (Fig. A3a) is:

$$A_0 = T(W + L)/2, \tag{A3.1a}$$

and the lost area of the graben in the compacted unit (Fig. A3b) is:

$$A_1 = (1 - C)T(W + L)/2, \tag{A3.1b}$$

where C is compaction as a fraction. Dividing Eq. (A3.1b) by Eq. (A3.1a) and solving for the original lost area gives:

$$A_0 = A_1/(1 - C), \tag{A3.2}$$

where the coefficient of A_1 will be called the decompaction ratio, $D.R.$ that is applied to the measured lost area to restore

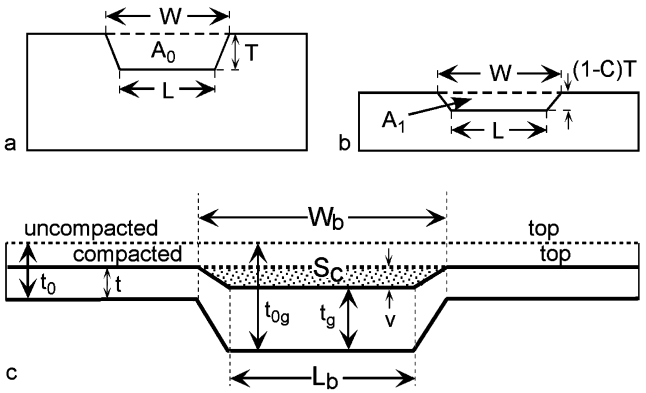

Fig. A3. Effects of compaction on a graben in a growth unit. (a) and (b) Graben in a thick compacting interval. A_0 = area of graben before compaction, W = width of graben at regional, L = width of graben at top of hanging wall, T = original depth of graben, A_1 = area of graben after compaction, C = fractional compaction. (a) Before compaction. (b) After compaction. (c) Differential compaction of growth graben. S_c = lost area of differential compaction (shaded); t and t_0 = compacted and original thicknesses outside the graben, respectively; t_g and t_{0g} = compacted and original thicknesses inside the graben, respectively; v = vertical dimension of differential compaction; W_b = width of graben between hanging wall cutoffs of the base of unit, L_b = maximum width of graben at base of unit.

it to its pre-compaction area:

$$D.R. = 1/(1 - C). \tag{A3.3}$$

Compaction of the thicker growth sequence in the graben (Fig. A3c) results in a lost area of differential compaction, S_c. The thicknesses after compaction outside and inside the graben are, respectively:

$$t = (1 - C)t_0, \tag{A3.4a}$$

$$t_g = (1 - C)t_{0g}, \tag{A3.4b}$$

where t and t_0 are compacted and uncompacted thicknesses, respectively, outside the graben and t_g and t_{0g} are compacted and uncompacted thicknesses, respectively, inside the graben. The vertical dimension of the lost area of differential compaction, v, is:

$$v = \Delta g - \Delta h = (t_g - t)(C/(1 - C)), \tag{A3.5}$$

where $\Delta g = t_{0g} - t_g$ and $\Delta h = t_0 - t$. The lost area of differential compaction is then:

$$S_c = v(L_b - W_b)/2, \tag{A3.6}$$

where L_b is the maximum width of the graben at the base of the unit and W_b is the width of the graben between hanging wall cutoffs of the base of the unit, and v is given by Eq. (A3.5). The lost area of differential compaction (Eq. (A3.6)) must be removed from the total displaced area to find the amount of displaced area caused by extension or contraction alone. If t_g is not constant, then the average value should provide a good estimate.

The fractional compaction, C, is given by:

$$C = 1 - [(1 - \phi_0)/(1 - \phi_1)]. \tag{A3.7}$$

where ϕ_1 is final porosity and ϕ_0 is initial porosity. If the final porosity is unknown, it can be estimated from the Rubey and Hubbert (1959) exponential compaction curve:

$$\phi_1 = \phi_0 e^{-cz}. \quad \text{(A3.8)}$$

where z is depth and c is compaction coefficient. The values of c and ϕ_0 are determined from compaction curves (e.g. Sclater and Christie, 1980).

References

Baxter, K., 1998. The role of small-scale extensional faulting in the evolution of basin geometries. An example from the Late Paleozoic Petrel sub-basin, northwest Australia. Tectonophysics 287, 21–41.

Bolin, D.E., Mann, S.D., Burroughs, D., Moore, H.E., Jr., Powers, T.J., 1989. Petroleum atlas of southwestern Alabama. Alabama Geological Survey Atlas 23.

Braunstein, J., 1953. Fracture-controlled production in Gilbertown Field, Alabama. American Association of Petroleum Geologists Bulletin 37, 245–249.

Brooks, B.A., Allmendinger, R.W., de la Barra, I.G., 1996. Fault spacing in the El Teniente mine, central Chile: evidence for nonfractal fault geometry. Journal of Geophysical Research 101, 13,633–13,653.

Carter, K.E., Winter, C.L., 1995. Fractal nature and scaling of normal faults in the Espanola Basin, Rio Grande rift, New Mexico: implications for fault growth and brittle strain. Journal of Structural Geology 17, 863–873.

Chai, B., 1994. Test of geometric models relating normal fault shape to rollover geometry in listric normal fault sandbox experiment. M.S. Thesis, University of Alabama.

Chai, B., Groshong, R.H. Jr, 1994. Test of cross-section balancing and restoring on experimental constant-displacement normal fault (abst.). American Association of Petroleum Geologists 1994 Annual Convention Program 3, 119.

Chamberlain, R.T., 1910. The Appalachian folds of central Pennsylvania. Journal of Geology 18, 228–251.

Childs, C., Walsh, J.J., Watterson, J., 1990. A method for estimation of the density of fault displacements below the limits of seismic resolution in reservoir formations. In: Bueller, A.T., (Ed.), North Sea Oil and Gas Reservoirs, II. The Norwegian Institute of Technology, Graham & Trotman, London, pp. 308–318.

Cloos, E., 1968. Experimental analysis of Gulf Coast fracture patterns. American Association of Petroleum Geologists Bulletin 52, 420–444.

Current, A.M., 1948. Gilbertown Field, Choctaw County, Alabama. Structure of Typical American Oil Fields. American Association of Petroleum Geologists, Tulsa, Oklahoma 3, pp. 1–4.

Ellevset, S.O., Knipe, R.J., Olsen, T.S., Fisher, Q.J., Jones, G., 1998. Fault controlled communication in the Sleipner Vest Field, Norwegian Continental Shelf; detailed, quantitative input for reservoir simulation and well planning. In: Jones, G., Fisher, Q.J., Knipe, R.J. (Eds.), Faulting, Fault Scaling, Fault Sealing and Fluid Flow in Hydrocarbon Reservoirs. Geological Society, London, Special Publication 147, pp. 283–297.

Epard, J.-L., Groshong, R.H. Jr, 1993. Excess area and depth to detachment. American Association of Petroleum Geologists Bulletin 77, 1291–1302.

Foley, L., Daltaban, T.S., Wang, J.T., 1998. Numerical simulation of fluid flow in complex faulted region. In: Coward, M.P., Daltaban, T.S., Johnson, H. (Eds.), Structural Geology in Reservoir Characterization. Geological Society, London, Special Publication 127, pp. 121–132.

Gibbs, A.D., 1983. Balanced cross-sections constructed from seismic sections in areas of extensional tectonics. Journal of Structural Geology 5, 153–160.

Groshong, R.H. Jr, 1990. Unique determination of normal fault shape from hanging-wall bed geometry in detached half grabens. Eclogae Geologicae Helvetiae 83, 455–471.

Groshong, R.H. Jr, 1994. Area balance, depth to detachment and strain in extension. Tectonics 13, 1488–1497.

Groshong, R.H., Jr, 1996. Construction and validation of extensional cross-sections using lost area and strain, with application to the Rhine graben. In: Buchanan, P.G., Nieuwland, D.A. (Eds.), Modern Developments in Structural Interpretation, Validation, and Modeling. Geological Society, London, Special Publication 199, pp. 79–87.

Groshong, R.H. Jr, 1999. 3-D Structural Geology, Springer-Verlag, Berlin.

Groshong, R.H. Jr, Epard, J.-L., 1994. The role of strain in area-constant detachment folding. Journal of Structural Geology 15, 613–618.

Groshong, R.H. Jr, Epard, J.-L., 1996. Computerized cross-section balance and restoration. In: DePaor, D.G., (Ed.), Structural Geology and Personal Computers, Pergamon Press, New York, pp. 477–498.

Groshong, R.H., Jr, Pashin, J.C., 1997. Predicting fractures from area-balanced cross-sections. Oral presentation at AAPG Hedberg Research Conference on Reservoir-Scale Deformation—Characterization and Prediction.

Groshong, R.H. Jr, Pashin, J.C., Schneeflock, R.D., 2001. Sub-resolution fault strain in a Gulf of Mexico growth graben: predictions from area balance confirmed by 3-D seismic (abst.). 2001 American Association of Petroleum Geologists Annual Convention Program Book A75.

Gross, M.R., Gutiérrez-Alonso, G., Bai, T., Wacker, M.A., Collinsworth, K.B., Behl, R.J., 1997. Influence of mechanical stratigraphy and kinematics on fault scaling relations. Journal of Structural Geology 19, 171–183.

Hansen, W.R., 1965. Effects of the earthquake of March 27, 1964, at Anchorage, Alaska. U.S. Geological Survey Professional Paper 542-A.

Hossack, J.R., 1979. The use of balanced cross-sections in the calculation of orogenic contraction: a review. Journal of the Geological Society of London 136, 705–711.

Jin, G., Groshong, R.H. Jr, Pashin, J.C., 1999. Relationship between drag fold geometry and fracture production in the Selma Chalk, Gilbertown oil field, southwest Alabama. Gulf Coast Association of Geological Societies Transactions 49, 17–18.

Kautz, S.A., Sclater, J.G., 1988. Internal deformation in clay models of extension by block faulting. Tectonics 7, 823–832.

King, G., 1983. The accommodation of large strains in the upper lithosphere of the Earth and other solids by self-similar fault systems: the geometrical origin of β-value. Pure and Applied Geophysics 121, 761–815.

King, G., Cisternas, A., 1991. Do little things matter? Nature 351, 350.

Knai, T.A., Knipe, R.J., 1998. The impact of faults on fluid flow in the Heidrun Field. In: Jones, G., Fisher, Q.J., Knipe, R.J. (Eds.), Faulting, Fault Scaling, Fault Sealing and Fluid Flow in Hydrocarbon Reservoirs. Geological Society, London, Special Publication 147, pp. 269–282.

Maerten, L., Pollard, D.D., Karpuz, R., 2000. How to constrain 3-D fault continuity and linkage using reflection seismic data: a geomechanical approach. American Association of Petroleum Geologists Bulletin 84, 1311–1324.

Manzocchi, T., Ringrose, P.S., Underhill, J.R., 1998. Flow through fault systems in high-porosity sandstones. In: Coward, M.P., Daltaban, T.S., Johnson, H. (Eds.), Structural Geology in Reservoir Characterization. Geological Society, London, Special Publication 127, pp. 65–82.

Marrett, R., Allmendinger, R.W., 1991. Estimates of strain due to brittle faulting: sampling of fault populations. Journal of Structural Geology 13, 735–738.

Marrett, R., Allmendinger, R.W., 1992. Amount of extension on "small" faults: an example from the Viking graben. Geology 20, 47–50.

McClay, K.R., 1992. Glossary of thrust tectonics terms. In: McClay, K.R., (Ed.), Thrust Tectonics, Chapman and Hall, London, pp. 419–433.

McClay, K.R., Ellis, P.G., 1987. Geometries of extensional fault systems developed in model experiments. Geology 15, 341–344.

Nicol, A., Walsh, J.J., Watterson, J., Gillespie, P.A., 1996. Fault size

distributions—are they really power law? Journal of Structural Geology 18, 191–197.

Pashin, J.C., Raymond, D.E., Alabi, G.G., Groshong, R.H. Jr, Jin, G., 2000. Revitalizing Gilbertown oil field: characterization of fractured chalk and glauconitic sandstone in an extensional fault system. Geological Survey of Alabama Bulletin 168.

Peacock, D.C.P., Sanderson, D.J., 1994. Strain and scaling of faults in the chalk at Flamborough Head, UK. Journal of Structural Geology 16, 97–107.

Rubey, W.W., Hubbert, M.K., 1959. Role of fluid pressure in mechanics of overthrust faulting II. Geological Society of America Bulletin 70, 167–206.

Scholz, C.H., Cowie, P.A., 1990. Determination of total strain from faulting using slip measurements. Nature 346, 837–839.

Sclater, J.G., Christie, P.A.F., 1980. Continental stretching: an explanation of the post-mid-Cretaceous subsidence of the central North Sea basin. Journal of Geophysical Research 85, 3711–3739.

Walsh, J.J., Watterson, J., Yielding, G., 1991. The importance of small-scale faulting in regional extension. Nature 351, 391–393.

Walsh, J.J., Watterson, J., Heath, A., Gillespie, P.A., Childs, C., 1998. Assessment of the effects of sub-seismic faults on bulk permeabilities of reservoir sequences. In: Coward, M.P., Daltaban, T.S., Johnson, H. (Eds.), Structural Geology in Reservoir Characterization. Geological Society, London, Special Publication 127, pp. 99–114.

White, N.J., Jackson, J.A., McKenzie, D.P., 1986. The relationship between the geometry of normal faults and that of the sedimentary layers in their hanging walls. Journal of Structural Geology 8, 897–909.

Wickham, J., Moeckel, G., 1997. Restorations of structural cross-sections. Journal of Structural Geology 19, 975–986.

Withjack, M.O., Islam, Q.T., La Pointe, P.R., 1995. Normal faults and their hanging wall deformation: an experimental study. American Association of Petroleum Geologists Bulletin 79, 1–18.

Wojtal, S.F., 1994. Fault scaling laws and the temporal evolution of fault systems. Journal of Structural Geology 16, 603–612.

Wojtal, S.F., 1996. Changes in fault displacement populations related to linkages between faults. Journal of Structural Geology 18, 265–279.

Wu, S., 1993. Fractal strain distribution and its implication for cross-section balancing. Journal of Structural Geology 15, 1497–1507.